# Controlling Catenations, Properties and Relative Ring-Component Movements in Catenanes with Aromatic Fluorine Substituents†

**Roberto Ballardini,‡ Vincenzo Balzani,*,§ Alberto Credi,§ Christopher L. Brown,¶ Richard E. Gillard,¶ Marco Montalti,§ Douglas Philp,¶ J. Fraser Stoddart,*,¶,⊗ Margherita Venturi,§ Andrew J. P. White,⊥ Brian J. Williams,|| and David J. Williams*,⊥**

*Contribution from The School of Chemistry, The University of Birmingham, Edgbaston, Birmingham B15 2TT, UK, Department of Chemistry, Imperial College, South Kensington, London SW7 2AY, UK, Merck Sharp & Dohme Research Laboratories, Neuroscience Research Centre, Terlings Park, Harlow CM20 2QR, UK, Dipartimento di Chimica "G. Ciamician" dell'Università, via Selmi 2, I-40126 Bologna, Italy, and Istituto FRAE-CNR, via Gobetti 101, I-40129 Bologna, Italy*

*Received February 27, 1997. Revised Manuscript Received October 16, 1997*⊗

**Abstract:** Four new fluorine-containing macrocyclic polyethers based on bis-*p*-phenylene-34-crown-10 have been synthesized and subsequently catenated, separately, with cyclobis(paraquat-*p*-phenylene). The efficiencies of the catenations are strongly influenced by the aromatic ring templates in the macrocyclic polyethers. Incorporation of fluorine atom substituents into one of the hydroquinone rings in bis-*p*-phenylene-34-crown-10 had only a small effect on the percentage yields, whereas employing bis-*p*-phenylene-34-crown-10 derivatives, in which both hydroquinone rings have been at least partially fluorinated, resulted in a dramatic decrease in catenation yields. In [2]catenanes incorporating macrocyclic polyethers containing one hydroquinone and one fluorinated hydroquinone ring, in both the solution ($^1$H and $^{19}$F NMR, and UV−vis spectroscopies, electrochemical studies and molecular modeling) and solid (X-ray crystallography and molecular modeling) states, by far the major translational isomers observed were the ones with the hydroquinone ring located "inside" the cavity of the tetracationic cyclophane. The diminished strength of the noncovalent interactions arising as a result of aromatic fluorine substituents is also reflected in the rates of the movements of the two ring components (dynamic NMR spectroscopy). As well as their electron-withdrawing effect, the fluorine substituents have a pronounced effect (UV−vis spectroscopy, electrochemical studies and molecular modeling) on the geometry of the ArO−$CH_2$ bonds within the (fluorinated) hydroquinone rings.

## Introduction

Self-assembly[1] has become a well-established paradigm for the creation of large, highly ordered, and functioning molecular assemblies and supramolecular arrays. In order to progress beyond the realm of simple supramolecular chemistry[2] in the direction of well-defined nanometer-scale devices,[3] it is necessary to understand and then to influence the molecular recognition that occurs between the component parts of self-assembled structures and superstructures. Mechanically interlocked molecular compounds are ideal target structures to be constructed by template-directed synthesis.[1,4] Furthermore, catenanes, rotaxanes, and knots[5] have considerable potential for applications in materials science and electronics.[6]

The molecular recognition between $\pi$-electron-deficient aromatic units, *e.g.*, the paraquat dication,[7] and $\pi$-electron-rich aromatic rings, *e.g.* the hydroquinone ring,[8] has provided the inspiration for the self-assembly of a large number[5] of mechanically interlocked structures and intertwined superstructures. Considerable effort has gone into changing the nature of the $\pi$-electron acceptor[9] and donor[10] components in order to fine-tune the structure and function of a range of self-assembled molecular compounds. Here, we have sought, within the context of our "original" [2]catenane in which bis-*p*-phenylene-34-crown-10 is interlocked with cyclobis(paraquat-*p*-phenylene), *to reduce the $\pi$-electron-donating nature of the hydroquinone rings in the macrocyclic polyether components by incorporating*

† "Molecular Meccano", Part 22. For Part 21, see: Asakawa, M.; Ashton, P. R.; Hayes, W.; Janssen, H. M.; Meijer, E. W.; Menzer, S.; Pasini, D.; Stoddart, J. F.; White, A. J. P.; Williams, D. J. *J. Am. Chem. Soc*. in press.

‡ Istituto FRAE-CNR, Bologna.

§ Dipartimento di Chimica "G. Ciamician" dell'Università, Bologna.

¶ University of Birmingham.

⊥ Imperial College, London.

|| Merck Sharp & Dohme.

* Address for correspondence: Dr. J. F. Stoddart, Department of Chemistry and Biochemistry, University of California at Los Angeles, 405 Hilgard Avenue, Los Angeles, CA 90095.

⊗ Abstract published in *Advance ACS Abstracts,* December 15, 1997.

(1) Philp, D.; Stoddart, J. F. *Angew. Chem., Int. Ed. Engl.* **1996**, *35*, 1154−1196.

(2) Lehn, J.-M. *Supramolecular Chemistry−Concepts and Perspectives*; VCH: Weinheim, 1995.

(3) Gómez-López, M.; Preece, J. A.; Stoddart, J. F. *Nanotechnology* **1996**, *7*, 183−192.

(4) Hoss, R.; Vögtle, F. *Angew. Chem., Int. Ed. Engl.* **1994**, *33*, 375−384.

(5) Amabilino, D. B.; Stoddart, J. F. *Chem. Rev.* **1995**, *95*, 2725−2828.

(6) (a) Robinson, A. L. *Science* **1984**, 223, 267−268. (b) See also a special issue of Science: Engineering in a Small World: From Atomic Manipulation to Microfabrication. *Science* **1991**, *254*, 1269−1424.

(7) For examples of paraquat receptors, see: (a) Ashton, P. R.; Chrystal, E. J. T.; Mathias, J. P.; Parry, K. P.; Slawin, A. M. Z.; Spencer, N.; Stoddart, J. F.; Williams, D. J. *Tetrahedron Lett.* **1987**, *28*, 6367−6370. (b) Bernado, A. R.; Lu, T.; Córdova, E.; Zhang, L.; Gokel, G. W.; Kaifer, A. E. *J. Chem. Soc., Chem. Commun.* **1994**, 529−530. (c) Gunter, M. J.; Johnston, M. R.; Skelton, B. W.; White, A. H. *J. Chem. Soc., Perkin Trans. 1* **1994**, *116*, 1009−1018. (d) Schenning, A. P. H. J.; de Bruin, B.; Rowan, A. E.; Kooijman, H.; Spek, A. L.; Nolte, R. J. M. *Angew. Chem. Int. Ed. Engl.* **1995**, *34*, 2132−2134.

(8) Stoddart, J. F. *Pure Appl. Chem.* **1988**, *60*, 467−472.

S0002-7863(97)00640-9 CCC: $14.00 © 1997 American Chemical Society

*electron-withdrawing substituents into the rings.* We have chosen fluorine atom substituents on account of their size complementarity with hydrogen ($r_F$ = 1.35 Å, $r_H$ = 1.10 Å) and their drastically different electronic properties.[11] We thereby hope, not only to develop more building blocks with useful probes for our *molecular meccano*[12] set, but also to increase the level of fundamental understanding of the nature of the interactions[13] between aromatic units and hopefully be able to employ the knowledge gained to introduce a much higher level of control into the relative movements of the component parts of mechanically interlocked molecules, such as catenanes and rotaxanes.

## Results and Discussion

**Synthesis of the Macrocyclic Polyethers and Their Catenations.** The macrocyclic polyethers **7**−**11** were synthesized according to Scheme 1. The bistosylates **1**, **2**, and **3**, incorporating successively hydroquinone, tetrafluorohydroquinone, and 2,5-difluorohydroquinone rings, were reacted with either hydroquinone (**4**), tetrafluorohydroquinone (**5**), or 2,5-difluorohydroquinone (**6**) in the presence of cesium carbonate[14] under high dilution conditions to give the required macrocyclic polyethers, which were all used, separately, in the self-assembly of the [2]-catenanes (Scheme 2). All the catenations were carried out under the same conditions: 2.5 mol equiv of the macrocyclic polyether, 1.0 mol equiv of the salt **12**·2$PF_6$, and 1.1 mol equiv of 1,4-bis(bromomethyl)benzene (**13**) were dissolved in a minimum volume of dry MeCN (dry DMF was used for **18**·4$PF_6$ since **11** was insoluble in MeCN at room temperature) in a sealed flask. Where catenations were unsuccessful or low yielding, ultrahigh pressures[15] were employed.

**Scheme 1**

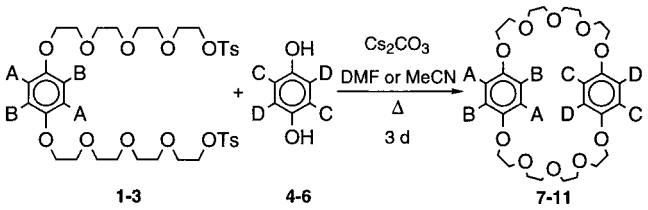


| Compound | A | B | C | D | %Yield |
|---|---|---|---|---|---|
| **1** | H | H | – | – | |
| **2** | F | F | – | – | |
| **3** | H | F | – | – | |
| **4** | – | – | H | H | |
| **5** | – | – | F | F | |
| **6** | – | – | H | F | |
| **7** | H | H | H | H | 15 |
| **8** | H | H | F | F | 14 |
| **9** | H | H | H | F | 12 |
| **10** | F | F | F | F | 23 |
| **11** | H | F | H | F | 43 |

**Scheme 2**

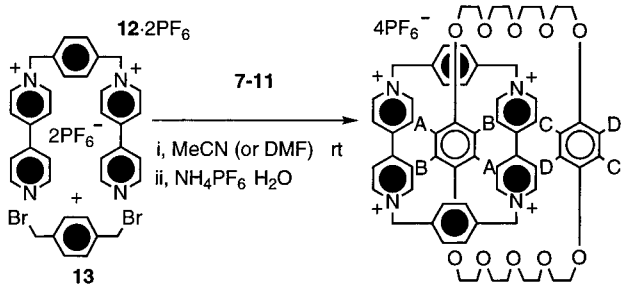


| Macrocycle | A | B | C | D | [2]Catenane | %Yield |
|---|---|---|---|---|---|---|
| **7** | H | H | H | H | **14**·4$PF_6$ | 70 |
| **8** | H | H | F | F | **15**·4$PF_6$ | 60 |
| **9** | H | H | H | F | **16**·4$PF_6$ | 57 |
| **10** | F | F | F | F | **17**·4$PF_6$ | 0 |
| **11** | H | F | H | F | **18**·4$PF_6$ | 3 |

The efficiencies of the catenations, reflected in the percentage yields, were found to be influenced strongly by the incorporation of fluorine atoms into the hydroquinone rings of the macrocyclic polyethers. The catenations, involving macrocyclic polyethers containing a hydroquinone ring and a fluorinated hydroquinone ring, either tetrafluorohydroquinone or 2,5-difluorohydroquinone, proceed in the relatively high yields of 60 and 57%, respectively, *cf.*, 70% for the self-assembly[16] of **14**·4$PF_6$. Using the macrocyclic polyethers containing two fluorinated hydroquinone rings results in dramatic drops in the yields of the corresponding [2]catenanes. The macrocyclic polyether **10**, incorporating two tetrafluorohydroquinone rings, does not template the formation of the [2]catenane **17**·4$PF_6$, even at 12 kbar. The catenation involving the macrocyclic polyether **11**, incorporating two 2,5-difluorohydroquinone rings as the aromatic ring templates, proceeded in only a 3% yield but was increased to 24% by ultrahigh pressures. These results are in accordance with binding studies carried out by $^1H$ and $^{19}F$ NMR

(9) (a) Ashton, P. R.; Ballardini, R.; Balzani, V.; Gandolfi, M. T.; Marquis, D. J.-F.; Pérez-García, L.; Prodi, L.; Stoddart, J. F.; Venturi, M. *J. Chem. Soc., Chem. Commun.* **1994**, 177−180. (b) Ashton, P. R.; Pérez-García, L.; Stoddart, J. F.; White, A. J. P.; Williams, D. J. *Angew. Chem., Int. Ed. Engl.* **1995**, *34*, 571−574. (c) Ashton, P. R.; Ballardini, R.; Balzani, V.; Credi, A.; Gandolfi, M. T.; Menzer, S.; Pérez-García, L.; Prodi, L.; Stoddart, J. F.; Venturi, M.; White, A. J. P.; Williams, D. J. *J. Am. Chem. Soc.* **1995**, *117*, 11171−11197. (d) Ballardini, R.; Balzani, V.; Credi, A.; Gandolfi, M. T.; Langford, S. J.; Menzer, S.; Prodi, L.; Stoddart, J. F.; Venturi, M.; Williams, D. J. *Angew. Chem., Int. Ed. Engl.* **1996**, *35*, 978−981.

(10) (a) Ashton, P. R.; Ballardini, R.; Balzani, V.; Blower, M.; Ciano, M.; Gandolfi, M. T.; Pérez-García, L.; Prodi, L.; McLean, C. H.; Philp, D.; Spencer, N.; Stoddart, J. F.; Tolley, M. S. *New J. Chem.* **1993**, *17*, 689−695. (b) Amabilino, D. B.; Ashton, P. R.; Brown, G. R.; Hayes, W.; Stoddart, J. F.; Tolley, M. S.; Williams, D. J. *J. Chem. Soc., Chem. Commun.* **1994**, 2479−2482. (c) Amabilino, D. B.; Dietrich-Buchecker, C. O.; Livoreil, A.; Pérez-García, L.; Sauvage, J.-P.; Stoddart, J. F. *J. Am. Chem. Soc.* **1996**, *118*, 3905−3913.

(11) (a) Pavlath, A. E.; Leffler, A. J. *Aromatic Fluorine Compounds*; ACS Monograph Series No. 155, Reinhold Publishing Corporation: London; 1961. (b) Tatlow, J. C. *Endeavour* **1963**, *22*, 89−95. (c) Sheppard, W. A. *J. Am. Chem. Soc.* **1970**, *92*, 5419−5422. (d) Chambers, R. D. *Chemistry of Organic Fluorine Compounds*, 2nd ed.; Wiley: New York, 1976. (e) Schlosser, M. *Tetrahedron* **1978**, *34*, 3−17. (f) Gerstenberger, M. R. C.; Haas, A. *Angew. Chem., Int. Ed. Engl.* **1981**, *20*, 647−664. (g) Welch, J. T. *The Effects of Selective Fluorination on Reactivity in Organic and Bioorganic Chemistry*; Welch, J. T., Ed.; ACS Symposium Series 456; American Chemical Society: Washington, DC, 1991; pp 1−15.

(12) Anelli, P. L.; Ashton, P. R.; Ballardini, R.; Balzani, V.; Delgado, M.; Gandolfi, M. T.; Goodnow, T. T.; Kaifer, A. E.; Philp, D.; Pietraszkiewicz, M.; Prodi, L.; Reddington, M. V.; Slawin, A. M. Z.; Spencer, N.; Stoddart, J. F.; Vicent, C.; Williams, D. J. *J. Am. Chem. Soc.* **1992**, *114*, 193−218.

(13) For reports on aryl−aryl interactions, see: (a) Jorgensen, W. L.; Severance, D. L. *J. Am. Chem. Soc.* **1990**, *112*, 4768−4774. (b) Hunter, C. A. *Chem. Soc. Rev.* **1994**, *23*, 101−109. (c) Nishio, M.; Umezawa, Y.; Hirota, M.; Takeuchi, Y. *Tetrahedron* **1995**, *51*, 8665−8701. For reports on the influence of fluorine on aryl−aryl interactions, see: (d) Makriyannis, A.; Fesik, S. *J. Am. Chem. Soc.* **1982**, *104*, 6462−6463. (e) Williams, J. H.; Cockcroft, J. K.; Fitch, A. N. *Angew. Chem., Int. Ed. Engl.* **1992**, *31*, 1655−1657. (f) Laatikainen, R.; Ratilainen, J.; Sebastian, R.; Santa, H. *J. Am. Chem. Soc.* **1995**, *117*, 11006−11010. (g) Cozzi, F.; Ponzini, F.; Annunziata, R.; Cinquini, M.; Siegel, J. S. *Angew. Chem., Int. Ed. Engl.* **1995**, *34*, 1019−1020. (h) Hunter, C. A.; Kapteijn, G. M.; Koten, G.; Lu, X-J. *J. Chem. Soc., Faraday Trans.* **1995**, *91*, 2009−2015.

(14) For a review of the 'cesium effect' in the synthesis of macrocyclic compounds, see: Ostrowicki, A.; Koepp, E.; Vögtle, F. *Top. Curr. Chem.* **1991**, *161*, 37−67.

(15) Brown, C. L.; Philp, D.; Stoddart, J. F. *Synlett* **1991**, 462−464.

(16) Ashton, P. R.; Goodnow, T. T.; Kaifer, A. E.; Reddington, M. V.; Slawin, A. M. Z.; Spencer, N.; Stoddart, J. F.; Vicent, C.; Williams, D. J. *Angew. Chem., Int. Ed. Engl.* **1989**, *28*, 1396−1399.

**Scheme 3**

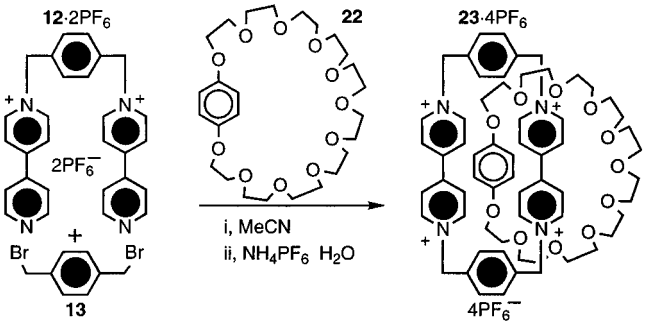


spectroscopies ($CD_3CN$ at 298 K) on the acyclic polyethers 1,2,4,5-tetrafluoro-3,6-bis[2-(2-hydroxyethoxy)ethoxy]benzene (**19**) and 1,4-difluoro-2,5-bis[2-(2-hydroxyethoxy)ethoxy]-benzene (**21**), and cyclobis(paraquat-*p*-phenylene) tetrakis-(hexafluorophosphate) (**20**·4$PF_6$). No complex formation was observed between the tetrafluorohydroquinone-containing "thread" and the tetracationic cyclophane. However, the tetracationic cyclophane bound the 2,5-difluorohydroquinone-containing "thread" weakly to form a pale orange complex ($K_a$ = 15 $M^{-1}$).[17] By comparison, 1,4-bis[2-(2-hydroxyethoxy)ethoxy]-benzene forms[12] a much stronger complex with the tetracationic cyclophane ($K_a$ = 2220 $M^{-1}$).

In the knowledge that a macrocyclic polyether (*e.g.*, **8** or **9**), in which one of the recognition sites has been effectively "switched off" by incorporation of fluorine atoms into the hydroquinone ring, can still template the formation of a [2]catenane (*i.e.*, **15**·4$PF_6$ or **16**·4$PF_6$) in high yield, we wished to test whether or not the second aromatic unit in the macrocyclic polyether was necessary for successful catenation. We prepared the ansa macrocyclic polyether **22**, containing only one aromatic unit in 15% yield by reacting the bistosylate **1** with diethylene glycol in the presence of NaH. The catenation of **22** with cyclobis(paraquat-*p*-phenylene) proceeds to give the [2]catenane **23**·4$PF_6$ (Scheme 3), but with a much reduced (8%) yield,[18] compared to the self-assembly[16] in 70% yield of the [2]catenane **14**·4$PF_6$.

**X-ray Crystallographic Characterization.** The X-ray structures of **8**, **9**, **15**·4$PF_6$, **16**·4$PF_6$, and **18**·4$PF_6$ have been determined. In that of **8** (Figure 1a), the principal features of interest are[19] (i) pronounced out-of-plane twisting and *anti* disposition of the $OCH_2$ bonds associated with the tetrafluorohydroquinone ring compared to an essentially planar arrangement for those bonds with the hydroquinone ring, (ii) self-filling of the macrocycle, and (iii) the tetrafluorohydroquinone and hydroquinone rings overlaying each other which are distinctly not parallel. Compound **9** (Figure 1b) crystallizes in a centrosymmetric space group, with the requirement that molecules possess a center of inversion. Clearly, this situation cannot exist and so the structure is disordered with the 2,5-difluorohydroquinone ring occupying the position of the hydroquinone ring in the lattice and *vice versa* in an evenly distributed fashion throughout the crystal. The macrocycle, like **8**, is self-filling; however, in **9**, the hydroquinone and 2,5-difluorohydroquinone rings are parallel (mean interplanar separation of 3.62 Å, centroid−centroid distance of 4.54 Å). It is interesting to note

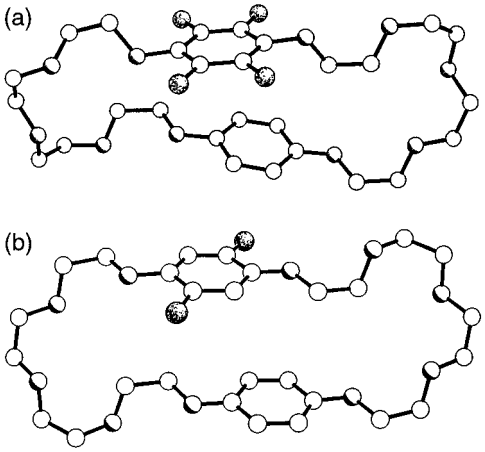


**Figure 1.** Ball-and-stick representations of the solid-state structures of (a) **8** (the rings are inclined by ∼16° and have a centroid−centroid separation of 4.27 Å), and (b) **9** (where the rings are parallel).

that, for both rings, their planes extend to include their adjacent *anti*-disposed $OCH_2CH_2$ units, *cf.*, the orthogonal arrangement for the tetrafluorohydroquinone ring in **8**. The molecules of both **8** and **9** form continuous $\pi-\pi$ stacks in the solid state.

The crystal structure (Figure 2a) of the tetrafluorohydroquinone-containing [2]catenane **15**·4$PF_6$ exhibits a pronounced perturbation of the normal $\pi$-donor/$\pi$-acceptor stacking motif. The tetrafluorohydroquinone ring, which is located "alongside" with respect to the tetracationic cyclophane, is tilted appreciably with respect to the "inside" bipyridinium unit. The centroid of the tetrafluorohydroquinone ring lies ∼4 Å from the mean plane of the "inside" bipyridinium unit. The [2]catenane is stabilized by the usual assemblage of $\pi-\pi$, C−H···$\pi$, and C−H···O interactions.[19]

In the structure of the [2]catenane **16**·4$PF_6$ incorporating **9** and cyclobis(paraquat-*p*-phenylene) the hydroquinone ring is positioned (Figure 2b) "inside" the cavity of the tetracationic cyclophane while the 2,5-difluorohydroquinone ring lies "alongside". The overall structure is little different from that of its non-fluorinated counterpart **14**·4$PF_6$, the only major difference being the adoption of an *anti* geometry by the $OCH_2$ bonds associated with the "alongside" 2,5-difluorohydroquinone ring, *cf.*, the *syn* geometry adopted by these $OCH_2$ bonds in the comparable hydroquinone ring in **14**·4$PF_6$. The only non-$\pi-\pi$-stacking interactions between the component rings of the [2]-catenane are of the T-type between the "inside" hydroquinone ring of the macrocyclic polyether and the *p*-phenylene rings of the tetracationic cyclophane. The H···$\pi$ distances and C−H···$\pi$ angles are 2.81 Å, 162° and 2.99 Å, 154°.

The [2]catenane **18**·4$PF_6$ in which both of the hydroquinone rings are 2,5-difluoro substituted has a solid-state structure (Figure 2c) that is virtually identical, even down to the unit cell dimensions, to that of **16**·4$PF_6$. Interestingly, despite the potential for the presence of different isomeric forms, in which the "inside" and "alongside" 2,5-difluorohydroquinone rings are either eclipsed or staggered with respect to one another, the crystals contain only the eclipsed isomer (and its enantiomer). At first sight, the most surprising feature of the structure is the directing of the C−F bonds of the "inside" 2,5-difluorohydroquinone ring into the $\pi$ faces of the *p*-phenylene rings of the tetracationic cyclophane. The associated F···$\pi$ distances and C−F···$\pi$ angles are 2.74 Å, 148° and 2.71 Å, 153°. The orientation of the "inside" 2,5-difluorohydroquinone ring is a direct consequence of the Ar−$OCH_2$ bonds being (i) coplanar with respect to the hydroquinone ring and (ii) *anti* to the fluorine atoms in each case. *Directing the C−F bonds into the $\pi$ faces*

(17) The binding constant was determined by an $^1H$ NMR dilution experiment.

(18) A macrocyclic polyether of similar size to bis-*p*-phenylene-34-crown-10 but with no aromatic units, *i.e.* 36-crown-12, is unable to template the formation of a [2]catenane with cyclobis(paraquat-*p*-phenylene), as the other ring component, either at ambient or ultrahigh pressure.

(19) Gillard, R. E.; Stoddart, J. F.; White, A. J. P.; Williams, B. J.; Williams, D. J. *J. Org. Chem.* **1996**, *61*, 4504−4505.

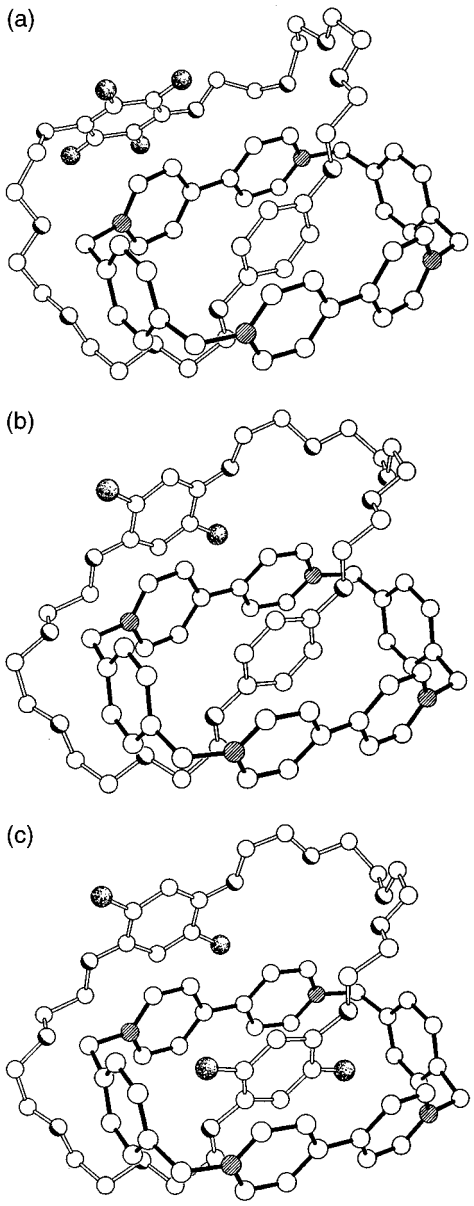


**Figure 2.** Ball-and-stick representations of the solid-state structures of the [2]catenanes (a) **15**·4$PF_6$, (b) **16**·4$PF_6$, and (c) **18**·4$PF_6$.

*of the p-phenylene rings is the only way both of these requirements can be satisfied*. This type of C−F···$\pi$ interaction[20] has been observed previously in other solid-state structures.[21] Apart from these particular intercomponent interactions, the only stabilizing factors are the normal face-to-face $\pi$ stacking between the $\pi$-electron-rich and -deficient ring systems. As in **16**·4$PF_6$, there are no C−H···O hydrogen bonding interactions in this [2]catenane.

**(Dynamic) NMR Spectroscopic Properties.** The solution-state properties of the [2]catenanes were investigated using variable-temperature $^1$H and $^{19}$F NMR spectroscopies in $CD_3CN$ and $CD_3COCD_3$. The relevant chemical shift data are summarized in Table 1. The associated kinetic and thermodynamic properties[22] for the dynamic processes taking place within the [2]catenanes are summarized in Table 2.

**Table 1.** $^1$H NMR (400 MHz) Chemical Shift Data [$\delta$ Values ($\Delta\delta$ Values)][a] for the [2]Catenanes Incorporating Bis-*p*-phenylene-34-crown-10 and Fluorinated Analogs, and Cyclobis(paraquat-*p*-phenylene) in $CD_3COCD_3$ Solution

| | charged component[b] | | | | polyether component[c] | |
|---|---|---|---|---|---|---|
| [2]catenane | α-CH | β-CH | $C_{6H4}$ | $CH_{2N}^+$ | ArH alongside | ArH inside |
| **14**·4$PF_6$ | 9.28 | 8.18 | 8.04 | 6.01 | 6.22 | 3.76 |
| | (−0.10) | (−0.40) | (+0.28) | (−0.14) | (−0.55) | (−3.01) |
| **15**·4$PF_6$ | 9.41 | 8.31 | 8.06 | 6.07 | −[d] | 3.75 |
| | (+0.03) | (−0.27) | (+0.30) | (−0.08) | −[e] | (−3.09) |
| **16**·4$PF_6$ | 9.35 | 8.26 | 8.06 | 6.04 | 6.39 | 3.99 |
| | (−0.03) | (−0.32) | (+0.30) | (−0.11) | (−0.59) | (−2.78) |
| **18**·4$PF_6$ | 9.33 | 8.29 | 7.99 | 6.03 | 6.40 | 5.08[f] |
| | (−0.05) | (−0.29) | (+0.23) | (−0.12) | (−0.58) | (−1.90) |
| **24**·4$PF_6$ | 9.39 | 8.29 | 8.07 | 6.07 | − | 3.88 |
| | (−0.01) | (−0.29) | (+0.31) | (−0.08) | − | (−2.89) |

[a] The $\Delta\delta$ values indicated in parentheses under the respective $\delta$ values relate to the changes in chemical shift exhibited by the probe protons upon catenane formation. A negative indicates the movement of the resonance to high field. [b] The $\delta$ values for the cyclobis(paraquat-*p*-phenylene) component in $CD_3COCD_3$ are 9.38, 8.58, 7.76, and 6.15 for the α-CH, β-CH, $C_6H_4$, and $CH_2N^+$ protons, respectively. [c] The $\delta$ values for the macrocyclic polyether components in $CD_3COCD_3$ are 6.77, 6.84, 6.98/6.77, 6.98, and 6.77 for the ArH protons of **14**·4$PF_6$, **15**·4$PF_6$, **16**·4$PF_6$, **18**·4$PF_6$, and **24**·4$PF_6$, respectively. [d] The $\delta_F$ value for the "alongside" tetrafluorohydroquinone ring is −156.9. [e] The $\delta_F$ value for the free macrocyclic polyether is −158.6. [f] At 233 K. The resonances are too broad to be observed at room temperature.

As a consequence of the introduction of different $\pi$ donors into the macrocyclic polyether component, the [2]catenanes **15**·4$PF_6$ and **16**·4$PF_6$ have the potential to undergo translational isomerism.[10] However, in $CD_3CN$ and $CD_3COCD_3$ solution, the only translational isomer of the [2]catenane **15**·4$PF_6$ which is observed is the one with the hydroquinone ring located "inside" the cavity of the tetracationic cyclophane, *i.e.*, the isomer observed in the solid state. The resonance ($\delta$ 3.75) for the protons on the hydroquinone ring appears in the shielded region of the $^1$H NMR spectrum, representing a shift of some 3.09 ppm upon catenane formation, *cf.*, a $\Delta\delta$ of −3.01 for **14**·4$PF_6$.

In the [2]catenane **16**·4$PF_6$, the major isomer[23] observed in both $CD_3CN$ and $CD_3COCD_3$ is also the one in which the hydroquinone ring, rather than the 2,5-difluorohydroquinone ring, is located "inside" the cavity of the tetracationic cyclophane. In the $^1$H NMR spectrum recorded in $CD_3COCD_3$, the resonances for the protons on the hydroquinone and 2,5-difluorohydroquinone rings occur at $\delta$ 3.99 (shielded) and $\delta$ 6.39 (deshielded), respectively.

The circumrotation (process I) of the macrocyclic polyether through the cavity of the tetracationic cyclophane could not be observed in either **15**·4$PF_6$ or **16**·4$PF_6$ by either $^1$H or $^{19}$F NMR spectroscopies. The circumrotation (process II) of the tetracationic cyclophane through the cavity of the macrocyclic polyether was observed and energy barriers of 11.4 and 12.2 kcal mol$^{-1}$ were obtained for **15**·4$PF_6$ and **16**·4$PF_6$, respectively, *cf.*, 12.2 kcal mol$^{-1}$ for **14**·4$PF_6$. These values are in accordance with earlier observations (*i.e.*, yields obtained in catenations, solid-state structures, $^1$H and $^{19}$F NMR spectroscopic data) which indicate that the interactions between both the hydroquinone

(20) Directing of the C−F bond into the $\pi$ face of the *p*-phenylene ring is not altogether surprising given the reluctance of organic fluorine, despite the high electronegativity of fluorine, to function as a hydrogen bond acceptor, see: Dunitz, J. D.; Taylor, R. *Chem. Eur. J.* **1997**, *3*, 89−98.

(21) (a) Dorau, A.; Mattes, R.; Teil, B. *Z. Naturforsch.* **1986**, *41*, 808−814. (b) Beaumont, C. A.; Brown, D. S.; Jones, J. B.; Massey, A. G.; Watkin, J. *J. Organomet. Chem.* **1988**, *344*, 1−8. (c) Bear, J. L.; Ham, B. C.; Kadish, K. M.; Li, Y. L. *Inorg. Chem.* **1993**, *32*, 4175−4176.

(22) The kinetic data were obtained by the coalescence method, where values of the rate constant ($k_c$) at the coalescence temperature ($T_c$) were obtained (Sutherland, I. O. *Annu. Rep. NMR Spectrosc.* **1971**, *4*, 71−235) from the approximate expression, $k_c = \pi(\Delta\upsilon)/(2)^{1/2}$, where $\Delta\upsilon$ is the limiting chemical shift difference (in hertz) between the exchanging proton resonances. The Eyring equation was then used to calculate $\Delta G^{\ddagger}_c$.

(23) An NMR saturation transfer experiment was performed in $CD_3CN$ solution at 303 K: it revealed that irradiation of a low intensity signal at $\delta$ 6.18 for the "alongside" hydroquinone ring protons leads to an enhancement of a signal at $\delta$ 3.75, for the "inside" hydroquinone ring protons.

**Table 2.** Kinetic and Thermodynamic Parameters Obtained from the Temperature-Dependent 400 MHz $^1$H NMR Spectra ($CD_3COCD_3$) Recorded on the [2]Catenanes Incorporating Bis-*p*-phenylene-34-crown-10 and some Fluorinated Analogs and Cyclobis(paraquat-*p*-phenylene)

| [2]catenane | process[a] | probe protons | $\Delta\nu$ (Hz) | $k_c$ ($s^{-1}$)[b] | $T_c$ (K)[b] | $\Delta G_c^{\ddagger}$ [b] (kcal $mol^{-1}$) |
|---|---|---|---|---|---|---|
| **14**·4$PF_6$ | I[c] | $OC_6H_4O$ | 678 | 1510 | 354 | 15.6 ± 0.2 |
| | II | α-CH | 74.3 | 165 | 250 | 12.0 ± 0.2 |
| | II | *β*-CH | 34.3 | 76 | 247 | 12.2 ± 0.2 |
| | II | $CH_2N^+$ | 45.8 | 102 | 248 | 12.1 ± 0.2 |
| **15**·4$PF_6$ | II | $C_6H_4$ | 52.7 | 117 | 235 | 11.4 ± 0.2 |
| | III | $CH_2N^+$ | 140 | 311 | 207 | 9.6 ± 0.2 |
| **16**·4$PF_6$ | II | α-CH | 38.0 | 84 | 247 | 12.2 ± 0.2 |
| | II | $CH_2N^+$ | 36.0 | 80 | 248 | 12.3 ± 0.2 |
| **18**·4$PF_6$ | I | $OC_6H_2F_2O$ | 535 | 1190 | 279 | 12.4 ± 0.2 |
| | II | α-CH | 67.0 | 149 | 240 | 11.6 ± 0.2 |
| | III | α-CH | 124 | 275 | 214 | 10.0 ± 0.2 |

[a] The dynamic processes taking place in these [2]catenanes are (i) the circumrotation of the macrocyclic polyether through the cavity of the tetracationic cyclophane (process I), which involves exchange of the "inside" and "alongside" hydroquinne rings, (ii) the circumrotation of the tetracationic cyclophane through the cavity of the macrocyclic polyether (process II), which involves exchange of the "inside" and "alongside" bipyridinium units, and (iii) the rocking (process III) of the "inside" hydroquinone ring within the cavity of the tetracationic cyclophane (see ref 12). [b] Determined by the coalescence method (see ref 22). [c] In $CD_3CN$.

and 2,5-difluorohydroquinone rings and the tetracationic cyclophane are stronger than the interaction of the tetrafluorohydroquinone ring with the tetracationic cyclophane.

The energy barrier for process I in the [2]catenane **18**·4$PF_6$ was determined to be 12.4 kcal $mol^{-1}$, some 3.2 kcal $mol^{-1}$ less than for the same process in **14**·4$PF_6$. This decrease in the activation energy for process I reflects a diminution in the molecular recognition between 2,5-difluorohydroquinone and the tetracationic cyclophane compared[24] with that of the hydroquinone ring.

**Molecular Modeling Studies.** Molecular modeling was carried out in an attempt to investigate the gross structural and dynamic changes observed in the [2]catenanes **15**·4$PF_6$ and **16**·4$PF_6$ that arise as a consequence of the incorporation of fluorine atoms into the hydroquinone rings of the macrocyclic polyether component.

An analysis of the molecular volumes of the hydroquinone ring and of the tetrafluorohydroquinone ring using Macromodel 5.0[25] afforded values of 91 and 106 Å$^3$, respectively, a volume increase that can be accommodated easily within the cavity of the tetracationic cyclophane. The relative energies for the two translational isomers—the structure of the unobserved translational isomer in which the tetrafluorohydroquinone ring is located "inside" the cavity of the tetracationic cyclophane was produced by molecular mechanics using structures generated from the X-ray crystal structure of **14**·4$PF_6$—derived from calculations performed both *in vacuo* and in water, employing both the GB/SA solvation[26] model and the AMBER* forcefield resident within Macromodel 5.0, suggest that the translational isomer in which the tetrafluorohydroquinone ring resides "alongside" the cavity of the tetracationic cyclophane, is appreciably lower in energy than the one in which the tetrafluorohydroquinone ring resides "inside". AM1 Semiempirical calculations, in which the minimized structures, obtained from molecular mechanics calculations, were used as starting-point structures, support these findings, suggesting that there is an energy penalty of some 4 kcal $mol^{-1}$ when the tetrafluorohydroquinone ring resides "inside" the cavity of the tetracationic cyclophane.

The C—H···$\pi$ (T-type) interaction is observed in many of the solid-state structures of this type:[12,27] Macromodel 5.0 predicts that, for a proton, the most stabilizing C—H···$\pi$ interaction occurs at a distance of 2.6−2.7 Å. However, in the case where the probe is a fluorine atom the optimum distance is found to be slightly larger at around 3.1 Å.

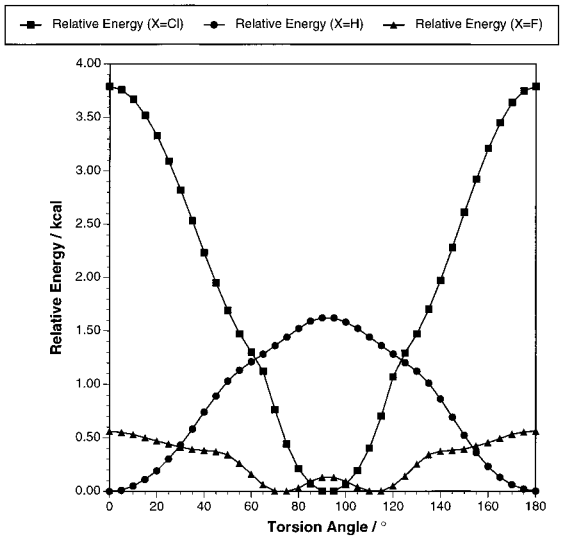


**Figure 3.** The potential energy curves described by torsion of the Ar−OMe bond in methoxybenzene, 1,3-difluoro-2-methoxybenzene, and 1,3-dichloro-2-methoxybenzene, calculated by AM1.

The X-ray crystal structures of the three macrocyclic polyethers **7**−**9** display an interesting pattern in the conformation adopted by the Ar-$OCH_2$ units, a pattern also present in the macrocyclic polyether component of the corresponding [2]-catenanes **14**·4$PF_6$−**16**·4$PF_6$. In the case of **7** and **9** (and of **14**·4$PF_6$ and **16**·4$PF_6$) the O−$CH_2$ bond lies in the plane of the aromatic ring, while in the case of **8** (and **15**·4$PF_6$), the O−$CH_2$ bond lies almost perpendicular to this plane. To probe this conformational preference, we examined three simple aryl methyl ethers where the substituents *ortho* to the OMe unit were H, F, or Cl. The Ar−OMe torsion angle was varied from 0 to 180° in 37 steps. The structure was allowed to relax through constrained geometry optimization and the energy of each conformation was calculated using AM1. Figure 3 illustrates the potential energy curves generated by these calculations. When X = H, there is significant stabilization associated with the placement of the O−Me bond in the plane of the aromatic ring. Hence, the observed torsion angles of 0 and 180° are

(24) This observation is reflected in the efficiency of the catenation process: 70% yield for **14**·4$PF_6$, and 3% for **18**·4$PF_6$ (25% at 12 kbar).

(25) Macromodel V5.0: Mohamadi, F.; Richards, N. G. J.; Guida, W. C.; Liskamp, R.; Lipton, M.; Caufield, C.; Chang, G.; Hendrickson, T.; Still, W. C. *J. Comput. Chem.* **1990**, *11*, 440−467.

(26) Still, W. C.; Tempczyk, A.; Hawley, R. C.; Hendrickson, T. *J. Am. Chem. Soc.* **1990**, *112*, 6127−6129.

(27) Asakawa, M.; Ashton, P. R.; Boyd, S. E.; Brown, C. L.; Gillard, R. E.; Kocian, O.; Raymo, F. M.; Stoddart, J. F.; Tolley, M. S.; White, A. J. P.; Williams, D. J. *J. Org. Chem.* **1997**, *62*, 26−37.

**Table 3.** Absorption and Emission Data in MeCN Solution at 298 K

| | absorption | | emission | | |
|---|---|---|---|---|---|
| compound | $\lambda_{max}$ (nm) | $\epsilon_{max}$ ($M^{-1}$ $cm^{-1}$) | $\lambda_{em}$ (nm) | $I_{rel}$[a] | $\tau$(ns)[b] |
| DMB[c] | 290 | 2600 | 324 | 100 | 2.5 |
| $F_2$-DMB | 283 | 2600 | 340 | 35 | 0.5 |
| $F_4$-DMB | 250(sh) | 470 | | | |
| | 283(sh) | 50 | | | |
| **7**[c] | 290 | 5200 | 320 | 70 | 2.0 |
| **8** | 290 | 2300 | 324 | 13 | <0.5 |
| **9** | 286 | 4500 | 324 | 50 | (d) |
| | | | 340 | 35 | (d) |
| **10** | 281(sh) | 470 | | | |
| | 248(sh) | 2000 | | | |
| 11 | 283 | 5200 | 340 | 35 | 0.5 |
| $\mathbf{14}^{4+}$ [c] | 263 | 36500 | | | |
| | 478 | 700 | | | |
| $\mathbf{15}^{4+}$ | 263 | 36000 | | | |
| | 473 | 370 | | | |
| $\mathbf{16}^{4+}$ | 264 | 39000 | | | |
| | 454 | 630 | | | |
| $\mathbf{18}^{4+}$ | 264 | 33000 | | | |
| | 424 | 500 | | | |
| $\mathbf{24}^{4+}$ | 262 | 37000 | | | |
| | 478 | 400 | | | |

[a] Relative emission intensity. [b] Excited states lifetime. [c] Already studied in ref 12. [d] Average lifetime ≈ 1.5 ns.

preferred. When X = Cl, there is significant steric repulsion associated with the placement of the O−Me bond in the plane of the aromatic ring as a result of the size of the Cl atoms in the 2- and 6-positions. Therefore, the most stable arrangement places the O−Me bond orthogonal to the plane of the aromatic ring in order to minimize these interactions. In the case of X = F, little conformational preference is observed. The size of the fluorine atom disfavors the conformation in which the O−Me unit is in the plane of the aromatic ring. However, the most stable arrangement does not place the O−Me unit orthogonal to this plane. It would therefore appear that the double-well potential observed when X = F is a result of a fine balance between two competing factors, stabilization by oxygen lone pair overlap with the aromatic $\pi$ system, and steric repulsion between the O−Me unit and the substituents (H, F, or Cl) in the 2- and 6-positions of the benzene ring. Since these two effects work in opposition to each other, they almost cancel out and give rise to the generally flat potential energy surface observed. Indeed, a search of the Cambridge Structural Database[28] reveals that of the eight structures suitable for comparison, the observed values for torsion angles range from 10 to 80°, indicating that there is little conformational preference being expressed in these systems.

**Absorption and Luminescence Properties.** The absorption and luminescence properties of the macrocyclic polyethers **8**−**11** and the [2]catenanes $\mathbf{15}^{4+}$, $\mathbf{16}^{4+}$, $\mathbf{18}^{4+}$, and $\mathbf{23}^{4+}$, as well as the reference compounds 1,4-dimethoxybenzene (DMB), 1,4-difluoro-2,5-dimethoxybenzene ($F_2$-DMB) and 1,2,4,5-tetrafluoro-3,6-dimethoxybenzene ($F_4$-DMB) in MeCN solution, have been investigated (Table 3).[29]

The absorption and emission spectra of $F_2$-DMB are similar to those of DMB except that (i) the Stokes shift is larger, (ii) the emission band is broader, (iii) the emission intensity is smaller, and (iv) the excited-state lifetime is shorter. These data suggest a larger molecular distortion upon excitation for $F_2$-DMB. The compound $F_4$-DMB exhibits a completely different absorption spectrum and does not show any emission. This difference can be related to the lack of a defined minimum energy conformation (Figure 3). A variety of conformers may be present, resulting in an absorption tail made of several closely lying bands. The much lower intensity could be related to the smaller overlap of the oxygen lone pairs with the $\pi$ system of the aromatic ring. The lower rigidity could also imply faster radiationless deactivation processes, which would account for the lack of emission.

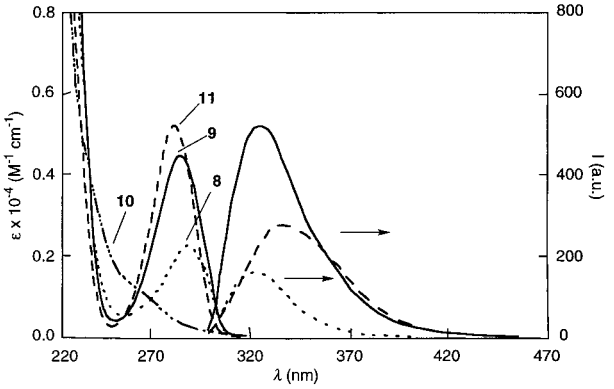


**Figure 4.** Absorption and emission spectra of the macrocyclic polyethers **8**−**11**.

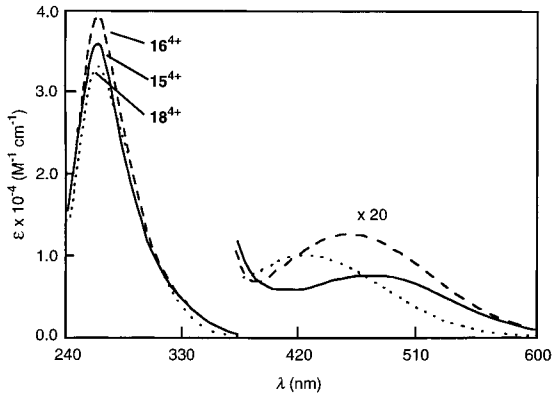


**Figure 5.** Absorption spectra of the [2]catenanes $\mathbf{15}^{4+}$, $\mathbf{16}^{4+}$, and $\mathbf{18}^{4+}$.

The absorption spectra (Figure 4) of the macrocyclic polyethers **8**−**11** are roughly what we would have expected from the spectra of the component chromophoric units. The emission properties (Figure 4) show that there is a weak interaction between these units. Macrocyclic polyether **9** shows a broad emission band which can be deconvoluted into two components corresponding to the bands of DMB and $F_2$-DMB. A quantitative analysis shows that the emission of the DMB-type unit is quenched by 50% with a corresponding sensitization of the $F_2$-DMB-type unit, *i.e.*, energy transfer occurs from the DMB- to the $F_2$-DMB-type unit. In macrocyclic polyether **8**, the luminescence intensity and lifetime of the DMB-type unit are reduced to 15% by a quenching process, which presumably involves energy transfer to the nonemissive $F_4$-DMB-type unit. Macrocyclic polyether **11** shows the emission of its $F_2$-DMB-type components, whereas macrocyclic polyether **10** shows no emission.

The absorption spectra of the [2]catenanes $\mathbf{15}^{4+}$, $\mathbf{16}^{4+}$, and $\mathbf{18}^{4+}$ are shown in Figure 5. Comparison with the sum of the spectra of the corresponding components shows an increase in the intensity of the tail of the strong UV absorption and the

(28) (a) Fletcher, D. A.; McMeeking, R. F.; Parkin, D. *Chem. Inf. Comput. Sci.* **1996**, *36*, 746−749. (b) Allen, F. H.; Kennard, O. *Chemical Design Automation News* **1993**, *8*, 1; 31−37.

(29) In this and the following sections, the aromatic rings in the macrocyclic polyethers are referred to as DMB-type units, preceded by the number of fluorine atoms attached to the ring (either $F_2$- or $F_4$-). We feel that this nomenclature system facilitates the comparison of the UV−vis spectroscopic and electrochemical properties of the macrocyclic polyethers and catenanes with those of the reference compounds.

**Table 4.** Electrochemical Data for the Reference Compounds, Macrocycles, and Related Catenanes[a]

| compound | $E_{1/2}^{red}$ | $E_{1/2}^{ox}$ |
|---|---|---|
| DMB | | +1.27[b] |
| $F_2$-DMB | | +1.46 |
| $F_4$-DMB | | +1.84 |
| **7** | | +1.23;[b] +1.36[b] |
| **11** | | +1.47[c] |
| **9** | | +1.27; +1.45 |
| **10** | | +1.85[c] |
| **8** | | +1.27; +1.85 |
| $\mathbf{20}^{4+}$ [d] | -0.29[c]; −0.71[c] | |
| $\mathbf{18}^{4+}$ | -0.21; −0.31; −0.80; −0.91 | +1.58; +1.82 |
| $\mathbf{16}^{4+}$ | -0.32; −0.39; −0.82; −0.91 | +1.57; +1.68 |
| $\mathbf{15}^{4+}$ | -0.31; −0.39; −0.85[c] | +1.64; +1.83 |
| $\mathbf{23}^{4+}$ | -0.31; −0.40; −0.84[c] | +1.58 |
| $\mathbf{14}^{4+}$ [d] | -0.31; −0.44; −0.84[c] | +1.42; +1.72 |

[a] Argon-purged MeCN solution, 298 K; halfwave potential values (in V) vs SCE; reversible and monoelectronic processes, unless otherwise noted. [b] Slightly different values are reported in ref 12. [c] Bielectronic process. [d] Data from ref 9c.

presence of a new broad but weak band in the visible region, characteristic of the CT interaction between $\pi$-donor and $\pi$-acceptor units. The absorption spectrum of $\mathbf{23}^{4+}$ (not shown in the figure) is, as expected, the same as that for the corresponding rotaxane,[12] incorporating a DMB-containing polyether and the $\mathbf{20}^{4+}$cyclophane. The charge-transfer absorption band of $\mathbf{16}^{4+}$ can be deconvoluted into two components resembling closely the CT bands of $\mathbf{23}^{4+}$ and (half that of) $\mathbf{18}^{4+}$. Subtracting the band of $\mathbf{23}^{4+}$ from that of $\mathbf{15}^{4+}$ yields an absorption band with $\lambda_{max} \sim 330$ nm on account of the interaction between a paraquat unit and the "alongside" $F_4$-DMB-type unit. In conclusion, each dimethoxybenzene-type unit undergoes a CT interaction with the paraquat units of the cyclobis(paraquat-*p*-phenylene) ring. The maximum of the corresponding band moves to higher energies along the series DMB-, $F_2$-DMB-, and $F_4$-DMB-type units, as expected from the potential values at which oxidation takes place (see Table 4). None of the [2]-catenanes shows any emission because of the presence of low energy CT levels.[12]

**Electrochemical Properties.** We also considered it important to study the electrochemical behavior of the [2]catenanes composed of the electron-acceptor tetracationic cyclophane $\mathbf{20}^{4+}$, whose electrochemical reduction has been extensively investigated,[12] and the four new electron-donor macrocyclic polyethers **8**−**11**. The reference compounds for the electroactive units which are present in the macrocycles are DMB, $F_2$-DMB, and $F_4$-DMB. In the potential window examined (−2.2/+2.2 V), each compound exhibits a reversible one-electron oxidation process whose potential becomes more positive as the number of fluorine atom substituents increases (Table 4, Figure 6). In the macrocyclic polyethers **8**−**11**, the two electroactive units behave in exactly the same way as those in the corresponding reference compounds, showing that the interaction between the units is negligible (Table 4). This behavior is in contrast with that of **7** where the two equivalent units are oxidized at different potentials, indicating the presence of some interaction that has also been evidenced by their spectroscopic measurements.[12]

*Oxidation Processes.* As a consequence of catenation, the two electroactive units of the macrocycles are more difficult to oxidize because they are engaged in donor−acceptor interactions (Table 4, Figure 6). Furthermore, they occupy topologically different positions ("inside" and "alongside" with respect to the tetracationic cyclophane). This, in the case of macrocycles containing two equivalent units, causes a splitting of the oxidation processes.

In catenane $\mathbf{18}^{4+}$, the oxidation (Figure 6) of the two $F_2$-DMB-type units, which, in the free macrocycle **11** simultaneously takes place at the potential of the $F_2$-DMB reference compound, occurs at more positive potentials and splits into two well-separated processes. The first oxidation process refers to the "alongside" unit, which experiences the effect of only one electron acceptor, and the second one, to the "inside" unit which is sandwiched between two electron acceptors. Such a behavior has previously been observed[12] for $\mathbf{14}^{4+}$: for a comparison, see Figure 6.

For catenanes $\mathbf{15}^{4+}$ and $\mathbf{16}^{4+}$, which contain nonsymmetric electroactive units, different electrochemical results are expected, depending on which translational isomer is present. In the case of $\mathbf{15}^{4+}$ (i) the first oxidation wave can be assigned to the DMB-type unit, considerably displaced toward more positive potentials because of the strong interaction associated with the "inside" position, and (ii) the second one is practically at the same potential as that of the $F_4$-DMB reference compound, showing that this unit lies in the "alongside" position. The assignment of the first oxidation process to an "inside" DMB-type unit is further supported by comparison with the behavior of $\mathbf{23}^{4+}$ (Figure 6). The translational isomer in which the $F_4$-DMB-type unit occupied the "inside" position and the DMB-type unit "alongside" would have exhibited the first oxidation wave at a potential close to that of the first wave of $\mathbf{14}^{4+}$. In conclusion, the electrochemical data not only confirm that the stable isomer is that with the DMB-type unit in the "inside" position, but also show that the $F_4$-DMB-type unit is substantially disengaged from any donor−acceptor interaction. For $\mathbf{16}^{4+}$ (Figure 6), the first oxidation process can be assigned to the "alongside" $F_2$-DMB-type unit by comparison with the first oxidation wave of $\mathbf{18}^{4+}$. The second wave can be assigned to the oxidation of the "inside" DMB-type unit by comparison with the first oxidation wave of $\mathbf{15}^{4+}$ and that of $\mathbf{23}^{4+}$. The displacement toward more positive potentials in $\mathbf{16}^{4+}$ is a consequence of the presence of an already oxidized unit. For the same reason, oxidation of the "inside" DMB-type unit of $\mathbf{14}^{4+}$ takes place at more positive potentials than it does for the "inside" DMB-type unit of $\mathbf{23}^{4+}$. It should also be noted that the translational isomer with the $F_2$-DMB-type unit in the "inside" position and the DMB-type unit in the "alongside" one would have exhibited a wave at much less positive potential (*i.e.*, close to that of the first wave of $\mathbf{14}^{4+}$) and a wave at much more positive potentials (*i.e.*, close to that of the second wave of $\mathbf{18}^{4+}$).

*Reduction Processes.* In the catenanes, the two equivalent electroactive units of the free tetracationic cyclophane $\mathbf{20}^{4+}$ are engaged in donor−acceptor interactions and occupy topologically different sites. Therefore, it can be expected that their reduction takes place at more negative potentials compared with free $\mathbf{20}^{4+}$, and in separated processes (Figure 6). This is clearly the case for $\mathbf{16}^{4+}$ which exhibits four reduction waves. The first and second waves (−0.32 and −0.39 V) can be assigned to the first reduction of the "alongside" and "inside" electron-acceptor units, respectively, and the third and fourth ones (−0.80 and −0.91 V) to the second reduction of the "alongside" and "inside" electron-acceptor units, respectively. A comparison with the behavior of the previously investigated[12] $\mathbf{14}^{4+}$ (Figure 6) shows that the first reduction occurs at the same potential in the two compounds because the "alongside" unit in both cases is engaged with a DMB-type unit. The second wave, corresponding to the first reduction of the "inside" electron acceptor unit, is more displaced toward negative potentials in $\mathbf{14}^{4+}$ compared to $\mathbf{16}^{4+}$ because, in the former, such a unit is sandwiched between two good electron donors. It should be noted that the second reduction of the two units occurs simultaneously at the same potential in $\mathbf{14}^{4+}$, whereas it occurs

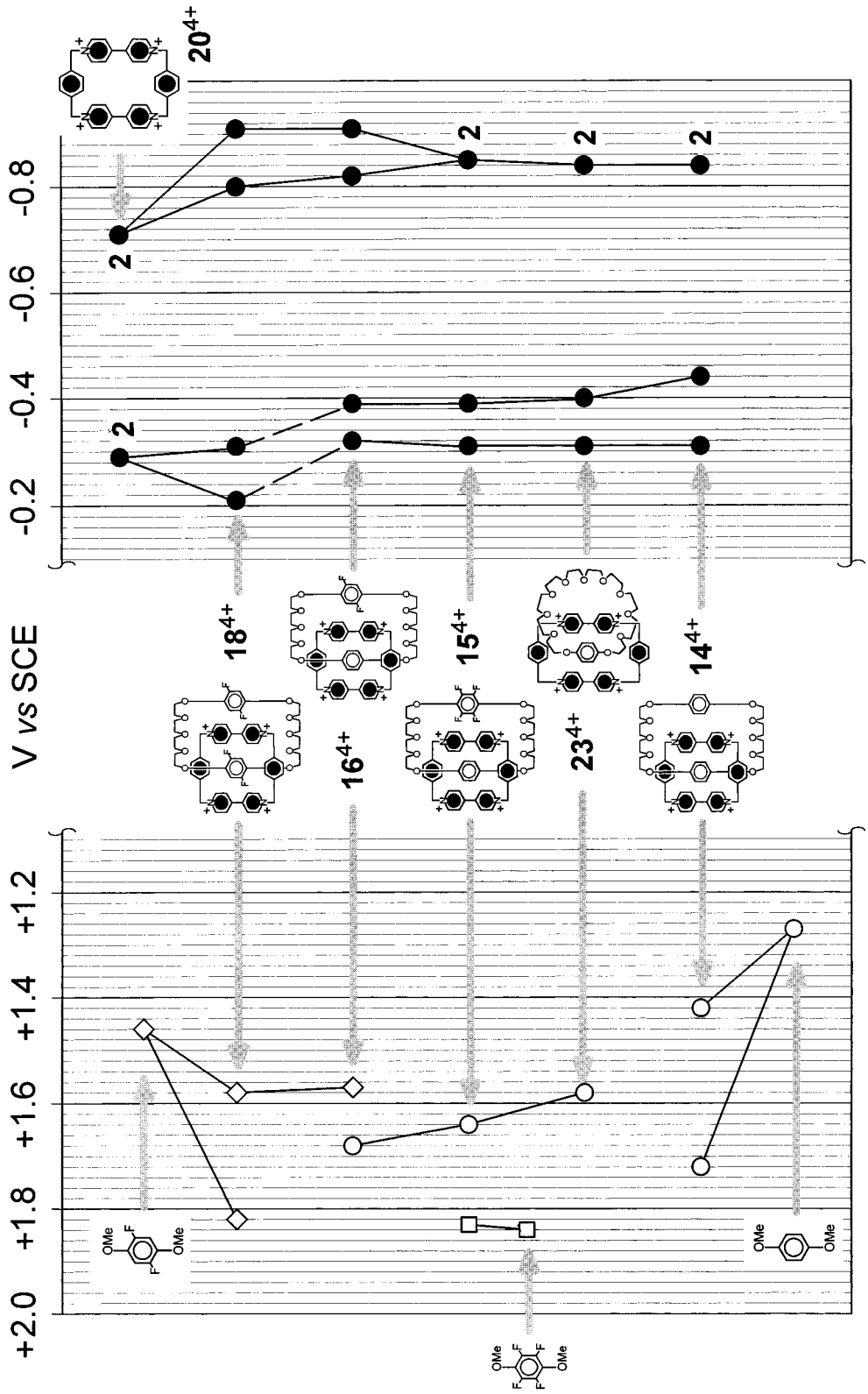


**Figure 6.** Correlations of the halfwave potentials for oxidation and reduction processes.

in separated steps in $\mathbf{16}^{4+}$. Clearly, after the first reduction, the "alongside"/"inside" distinction for the two electron-acceptor units, no longer valid in $\mathbf{14}^{4+}$, maintains some meaning in the case of $\mathbf{16}^{4+}$. It should also be noted that in $\mathbf{16}^{4+}$ the displacement toward more negative potentials compared to $\mathbf{20}^{4+}$ and the splitting between the potentials of the two units are larger for the second reduction (Figure 6). This observation indicates that, as previously observed for other catenanes,[9c] the reduction potentials are affected not only by donor-acceptor interactions, but also by structure-related factors. One such factor might be the degree of coplanarity of the two pyridine rings of the electron-acceptor units. It is well known, in fact, that reduction becomes easier as coplanarity is approached.[30] Catenation with macrocycles containing electron donors of different sizes and constitutions could play an important role in this respect (*vide infra*). The behavior of $\mathbf{15}^{4+}$ and $\mathbf{23}^{4+}$ is similar to that of $\mathbf{16}^{4+}$ in so far as the first reduction of the two units is concerned, and analogous to $\mathbf{14}^{4+}$ for the second reduction. Compound $\mathbf{18}^{4+}$ shows four reduction processes as in the case of $\mathbf{16}^{4+}$. As expected, because of the less pronounced electron-donor power of $F_2$-DMB compared to DMB, the first reduction of the two units takes place at potentials less negative than in the case of $\mathbf{16}^{4+}$. Surprisingly, however, the first process occurs at a potential which is also less negative than the simultaneous first reduction of the two equivalent units of the free cyclophane $\mathbf{20}^{4+}$. This result is unexpected because, as shown by the presence of a CT band and the displacement of the potentials at which oxidation of the electron-donor units of the macrocycle takes place, there is an electron donor−acceptor interaction in $\mathbf{18}^{4+}$. Clearly, other effects overcompensate for the expected displacement toward more negative potentials of the reduction processes caused by the donor−acceptor interaction. A possible influencing factor could be the very special structure of this catenane (*vide supra*), characterized by the O−$CH_2$ bonds of the Ar−$OCH_2$ units lying in the plane of the aromatic ring in an *anti* arrangement with respect to the fluorines. The X-ray structure shows that the two fluorine atoms on the "inside" $F_2$-DMB-type unit point into the faces of the *p*-phenylene spacers in the cyclophane. This arrangement could induce structural changes which favor coplanarity of the two pyridinium rings of the paraquat units and, thereby, facilitate their reduction. The assignment of the two reduction waves to the "inside" or "alongside" paraquat units of $\mathbf{18}^{4+}$ is not straightforward. According to the general trend observed for catenanes containing two equivalent electron-donor moieties in the macrocycle, one would expect the "alongside" unit to be reduced at a less negative potential than the "inside" one. However, one cannot exclude the possibility that the wave at less negative potential corresponds to reduction of the "inside" unit if both the $F_2$-DMB-type units are involved in forcing coplanarity of its pyridinium rings.

## Conclusions

It was our aim to reduce the $\pi$-electron donating nature of the hydroquinone rings in the macrocyclic polyether components of the prototypical [2]catenane $\mathbf{14}\cdot 4PF_6$ by incorporating electron-withdrawing (fluorine atom) substituents into them. The efficiencies of the catenations, as well as the structure and properties of the [2]catenanes formed were found to be influenced strongly by the fluorine atom substituents, as follows:

(1) Yields of catenations decrease with the introduction of fluorine atom substituents onto the hydroquinone rings. Note the 70, 60, 57, 3, and 0% yields of [2]catenanes in the case of $\mathbf{14}\cdot 4PF_6$, $\mathbf{15}\cdot 4PF_6$, $\mathbf{16}\cdot 4PF_6$, $\mathbf{18}\cdot 4PF_6$, and $\mathbf{17}\cdot 4PF_6$, respectively.

(30) Wardman, P. *J. Phys. Chem. Ref. Data* **1989**, *18*, 1637−1755.

(2) In both the solution and solid states, by far the major translational isomer has the hydroquinone ring located "inside" and the fluorinated hydroquinone ring "alongside" the tetracationic cyclophane. Note the 100:0 and 95:5 ratios, in $CD_3COCD_3$ solutions, in favor of the hydroquinone ring "inside" in the case of $\mathbf{15}\cdot 4PF_6$ and $\mathbf{16}\cdot 4PF_6$, respectively.

(3) The rates of the relative movements of the ring components increase as more and more fluorine atom substituents are added to the hydroquinone rings. This trend reflects the decrease in intercomponent interactions as more and more fluorine atom substituents replace the four aromatic hydrogen atoms.

(4) The orientation of the 2,5-difluorohydroquinone ring located "inside" the tetracationic cyclophane is a direct consequence of the desire of the two Ar-$OCH_2$ units to be coplanar with respect to the hydroquinone ring and *anti* in relation to the fluorine atoms.

This research represents a fine-tuning of the prototypical [2]catenane $\mathbf{14}\cdot 4PF_6$ to the extent that we have a unit which resides preferentially "alongside" the tetracationic cyclophane, but can, when forced, be accepted "inside" the cavity. These fluorinated derivatives are now being employed in the design of molecules that can be "switched" by some external stimulus.

## Experimental Section

**General Methods.** These have been described in previous parts of the series of papers (see, for example refs 9c and 12).

**2,5-Difluorohydroquinone (6).** 1,4-Difluoro-2,5-dimethoxybenzene (3.00 g, 17.2 mmol) dissolved in dry $CH_2Cl_2$ (20 mL) was added with stirring over a 5 min period to a stirred solution of $BBr_3$ (25.9 g, 104 mmol) in dry $CH_2Cl_2$ (104 mL) at −78 °C. The reaction mixture was allowed to warm up to room temperature and was stirred overnight, before being cooled to 0 °C and quenched with MeOH (30 mL) and then with $H_2O$ (10 mL). The solvent was removed and the residue was dissolved in EtOAc (100 ml) and washed with $H_2O$ (100 mL). The organic layer was dried ($MgSO_4$) and then concentrated to yield **6** as an off-white solid (2.48 g, 99%): mp 117.0−117.5 °C; EIMS *m/z* 146 [$M^+$]; $^1$H NMR ($CD_3COCD_3$, 300 MHz) $\delta$ 8.30 (2H, s), 6.77 (2H, m, $J_{HF}$ = 10 Hz); $^{19}$F NMR ($CDCl_3$, 280 MHz) $\delta_F$ −141.0 (s); $^{13}$C NMR ($CDCl_3$, 75 MHz) $\delta_C$ 147.6 (m, $J_{CF}$ = 237 Hz, $Ar_{CF}$), 137.9 (m, $Ar_{CO}$), 106.2 (m, $Ar_{CH}$); HRMS calcd for $[M]^+$ $C_6H_4F_2O_2$ 146.0179, found 146.0177.

**1,2,4,5-Tetrafluoro-3,6-dimethoxybenzene.** Methyl iodide (59.3 g, 0.42 mol) in dry degassed MeCN (50 mL) was added over a 1 h period to a previously degassed suspension of tetrafluorohydroquinone (7.60 g, 0.04 mol) and $K_2CO_3$ (57.6 g, 0.42 mol) in dry MeCN (80 mL) under $N_2$ with stirring. The reaction mixture was heated up to reflux and maintained at this temperature for 3 d. After cooling down to room temperature, the reaction mixture was filtered and the solvent was removed to leave an oily residue, which was dissolved in $CH_2Cl_2$ (200 mL) and washed with $H_2O$ (200 mL). The organic layer was dried ($MgSO_4$) and concentrated to a residue which was subjected to column chromatography ($SiO_2$, $CH_2Cl_2$/hexane 1:1) to give a yellow oil that was distilled under reduced pressure (∼1 mbar) using a Kugelrohr at 63 °C to yield the title compound as white needles (200 mg, 2%): EIMS *m/z* 210 $[M]^+$, 195 $[M - CH_3]^+$; $^1$H NMR ($CDCl_3$, 300 MHz) $\delta$ 4.02 (s); $^{19}$F NMR ($CDCl_3$, 280 MHz) $\delta_F$ −158.6 (s); HRMS calcd for $[M]^+$ $C_8H_6F_4O_2$ 210.0304, found 210.0305.

**1,2,4,5-Tetrafluoro-3,6-bis[2-[2-[2-[2-(*p*-toluenesulfonyl)ethoxy]-ethoxy]ethoxy]ethoxy]benzene (2).** Tetrafluorohydroquinone (6.00 g, 33.0 mmol) was added to a previously degassed suspension of $K_2CO_3$ (45.5 g, 329.7 mmol) and tetraethylene glycol monotosylate (23.0 g, 65.9 mmol) in dry DMF (400 mL) under $N_2$ with stirring. The reaction mixture was heated to 100 °C and stirred for 3 d. After cooling down to room temperature, the reaction mixture was filtered and the solvent was removed to leave a solid residue, which was dissolved in $CH_2Cl_2$ (250 mL) and washed with $H_2O$ (2 × 250 mL). The organic layer was dried ($MgSO_4$) and concentrated to a residue which was passed through $SiO_2$ ($CH_2Cl_2$/MeOH 100:3) to yield a brown oil. The brown

oil (5.53 g) was dissolved in $CH_2Cl_2$ (120 mL), along with $Et_3N$ (2.09 g, 20.71 mmol) and 4-(dimethylamino)pyridine (cat.), and cooled to 0 °C. A solution of *p*-toluenesulfonyl chloride (3.95 g, 20.71 mmol) in $CH_2Cl_2$ (80 mL) was added during 1 h and the reaction mixture stirred overnight. The solution was washed with 5% aqueous HCl (2 × 200 mL) and $H_2O$ (200 mL) and dried ($MgSO_4$). The solvent was removed, and the residue was purified by column chromatography ($SiO_2$, $CH_2Cl_2$/MeOH 50:1) to yield **2** as a colorless oil (6.98 g, 25%): FABMS *m/z* 843 $[M + H]^+$; $^1H$ NMR ($CDCl_3$, 300 MHz) $\delta$ 7.72 (4H, d, $J$ = 9 Hz), 7.30 (4H, d, $J$ = 9 Hz), 4.23 (4H, t), 4.10 (4H, t), 3.75 (4H, t), 3.50−3.67 (20H, m), 2.40 (6H, s); $^{19}F$ NMR ($CDCl_3$, 280 MHz) $\delta_F$ −158.6 (s); $^{13}C$ NMR ($CDCl_3$, 75 MHz) $\delta_C$ 144.8, 141.8 (m, $J_{CF}$ = 252 Hz, $Ar_{CF}$), 132.9 (m, $Ar_{CO}$), 132.9, 129.8, 127.8, 74.4, 70.7, 70.6, 70.5, 70.4, 70.1, 69.3, 68.5, 21.5; HRMS calcd for $[M + H]^+$ $C_{36}H_{47}F_4O_{14}S_2$ 843.2343, found 843.2328. Anal. Calcd for $C_{36}H_{46}F_4O_{14}S_2$: C 51.30, H 5.50; found C 51.39, H 5.34.

**1,4-Difluoro-2,5-bis[2-[2-[2-[2-(*p*-toluenesulfonyl)ethoxy]ethoxy]-ethoxy]ethoxy]benzene (3).** The procedure described for **2** was followed to yield **3** as a colorless oil (1.68 g, 5%): FABMS 807 $[M + H]^+$; $^1H$ NMR ($CDCl_3$, 300 MHz) $\delta$ 7.71 (4H, d, $J$ = 9 Hz), 7.34 (4H, d, $J$ = 9 Hz), 6.81 (2H, m, $J_{HF}$ = 10 Hz), 4.15 (8H, m), 3.83 (4H, t), 3.53−3.75 (20H, m), 2.43 (6H, s); $^{19}F$ NMR ($CDCl_3$, 280 MHz) $\delta_F$ −136.7 (s); $^{13}C$ NMR ($CDCl_3$, 75 MHz) $\delta_C$ 148.5 (m, $J_{CF}$ = 241 Hz, $Ar_{CF}$), 144.8, 140.6 (m, $Ar_{CO}$), 133.0, 129.8, 127.9, 105.3, 70.8, 70.7, 70.6, 70.5, 70.2, 69.6, 69.3, 68.6, 21.6; HRMS calcd for $[M]^+$ $C_{36}H_{48}F_2O_{14}S_2$ 806.2454, found 806.2465.

**1,2,4,5-Tetrafluoro-3,6-bis[2-(2-hydroxyethoxy)ethoxy]benzene (19).** A solution of tetrafluorohydroquinone (10.0 g, 55.0 mmol) in MeCN (40 mL) was added to a previously degassed suspension of $K_2CO_3$ (60.7 g, 439.6 mmol) and 2-(2-chloroethoxy)ethoxyethanol (20.5 g, 165 mmol) in dry MeCN (80 mL) under $N_2$ with stirring. The reaction mixture was heated to 60 °C and stirred for 7 d. After cooling down to room temperature, the reaction mixture was filtered and the solvent was removed to leave a solid residue which was dissolved in $CH_2Cl_2$ (200 mL) and washed with $H_2O$ (250 mL). The organic layer was dried ($MgSO_4$) and concentrated to a residue which was purified by column chromatography ($SiO_2$, $CH_2Cl_2$/MeOH 100:3) to yield **19** as a colorless oil (8.00 g, 40%): EIMS 358 $[M^+]$; $^1H$ NMR ($CDCl_3$, 300 MHz) $\delta$ 3.53−3.73 (16H, m), 3.00 (2H, t); $^{19}F$ NMR ($CDCl_3$, 280 MHz) $\delta_F$ −158.5 (s); $^{13}C$ NMR ($CDCl_3$, 75 MHz) $\delta_C$ 142.0 (m, $J_{CF}$ = 252 Hz, $Ar_{CF}$), 132.0 (m, $Ar_{CO}$), 72.3, 72.3, 70.9, 70.9. Anal. Calcd for $C_{14}H_{18}F_4O_6$: C 46.93, H 5.06; found C 46.96, H 4.96.

**1,4-Difluoro-2,5-bis[2-(2-hydroxyethoxy)ethoxy]benzene (21).** The procedure described for **19** was followed to yield **21** as a colorless oil (0.50 g, 6%): EIMS *m/z* 322 $[M^+]$; $^1H$ NMR ($CDCl_3$, 300 MHz) $\delta$ 7.08 (2H, m, $J_{HF}$ = 10 Hz), 4.20 (4H, t), 3.82 (4H, t), 3.55−3.70 (8H, m); $^{19}F$ NMR ($CDCl_3$, 280 MHz) $\delta_F$ −136.6 (s); $^{13}C$ NMR ($CDCl_3$, 75 MHz) $\delta_C$ 148.5 (m, $J_{CF}$ = 252 Hz, $Ar_{CF}$), 143.5 (m, $Ar_{CO}$), 105.5, 72.7, 72.4, 71.1, 70.2; HRMS calcd for $[M]^+$ $C_{14}H_{20}F_2O_6$ 322.1228, found 322.1233.

***p*-Phenylenetetrafluoro-*p*-phenylene-34-crown-10 (8).** Tetrafluorohydroquinone (0.76 g, 4.15 mmol) was added to a previously degassed suspension of $Cs_2CO_3$ (27.05 g, 83.04 mmol) and CsOTs (1.26 g, 4.15 mmol) in dry MeCN (400 mL) under $N_2$ with stirring. After the mixture was stirred at 80 °C for 1 h, a solution of **2** (3.33 g, 4.32 mmol) and CsOTs (1.26 g, 4.15 mmol) in dry, degassed MeCN (200 mL) was added dropwise over a 1 h period and heating was maintained for 5 d. After cooling to room temperature, the reaction mixture was filtered. The filtrate was collected and the solvent removed to leave a solid residue, which was dissolved in PhMe (200 mL) and washed with $H_2O$ (250 mL). The aqueous layer was washed with PhMe (3 × 100 mL). The organic layers were combined and dried ($MgSO_4$) and the solvent concentrated to a brown oil which was purified by column chromatography ($SiO_2$, $CH_2Cl_2$/MeOH 50:1), followed by recrystallization ($CHCl_3$/hexane) to yield **8** as a white crystalline solid (350 mg, 14%): mp 73.5−74.0 °C; FABMS *m/z* 608 $[M^+]$; $^1H$ NMR ($CDCl_3$, 300 MHz) $\delta$ 6.78 (4H, s), 4.20 (4H, t), 4.05 (4H, t), 3.80−3.86 (8H, m), 3.64−3.75 (16H, m); $^{19}F$ NMR ($CDCl_3$, 380 MHz) $\delta_F$ −158.60 (s); $^{13}C$ NMR ($CDCl_3$, 75 MHz) $\delta_C$ 149.7, 139.5 (m, $J_{CF}$ = 252 Hz, $Ar_{CF}$), 129.4 (m, $Ar_{CO}$), 111.9, 74.5, 70.8, 70.8, 70.8, 70.8, 70.1, 69.7, 68.2; HRMS calcd for $[M]^+$ $C_{28}H_{36}F_4O_{10}$ 608.2245, found 608.2230. Anal. Calcd for $C_{28}H_{36}F_4O_{10}$: C 55.26, H 5.90; found C 55.55, H 6.07.

***p*-Phenylene-2,5-difluoro-*p*-phenylene-34-crown-10 (9).** The procedure described for the preparation of **8** was followed to yield **9** as a white crystalline solid (290 mg, 12%): mp 84.0−84.5 °C; positive-ion ES MS *m/z* 590 $[M + NH_4]^+$; $^1H$ NMR ($CDCl_3$, 360 MHz) $\delta$ 6.77 (4H, s), 6.73 (2H, m, $J_{HF}$ = 10 Hz), 4.02 (8H, m), 3.83 (8H, m), 3.69 (16H, m); $^{19}F$ NMR ($CDCl_3$, 340 MHz) $\delta_F$ −133.1 (s); $^{13}C$ NMR ($CDCl_3$, 90 MHz) $\delta_C$ 153.1, 147.8 (m, $J_{CF}$ = 245 Hz, $Ar_{CF}$), 140.5 (m, $Ar_{CO}$), 115.6, 70.8, 70.8, 70.8, 70.7, 70.3, 69.7, 69.6, 68.2; HRMS calcd for $[M]^+$ $C_{28}H_{38}F_2O_{10}$ 572.2433, found 572.2421.

**Bis(tetrafluoro-*p*-phenylene)-34-crown-10 (10).** The procedure described for the preparation of **8** was followed to yield **10** as a white amorphous solid (115 mg, 23%): mp 72.0−73.0 °C; FABMS *m/z* 681 $[M + H]^+$; $^1H$ NMR ($CDCl_3$, 300 MHz) $\delta$ 4.27 (8H, m), 3.79 (8H, m), 3.55−3.68 (16H, m); $^{19}F$ NMR ($CDCl_3$, 340 MHz) $\delta_F$ −158.8 (s); $^{13}C$ NMR ($CDCl_3$, 90 MHz) $\delta_C$ 141.8 (m, $J_{CF}$ = 242 Hz, $Ar_{CF}$), 132.9 (m, $Ar_{CO}$), 74.4, 70.8, 70.7, 70.2; HRMS calcd for $[M]^+$ $C_{28}H_{32}F_8O_{10}$ 680.1868, found 608.1876.

**Bis(2,5-difluoro-*p*-phenylene)-34-crown-10 (11).** The procedure described for the preparation of **8** was followed to yield **11** as a white crystalline solid (482 mg, 43%): mp 127.0−127.5 °C; FABMS *m/z* 741 $[M + Cs]^+$, 608 $[M^+]$; $^1H$ NMR ($CDCl_3$, 300 MHz) $\delta$ 6.79 (4H, m, $J_{HF}$ = 10 Hz), 4.11 (8H, t), 3.86 (8H, t), 3.70 (16H, m); $^{19}F$ NMR ($CDCl_3$, 280 MHz) $\delta_F$ −136.7 (s); $^{13}C$ NMR ($CDCl_3$, 75 MHz) $\delta_C$ 148.1 (m, $J_{CF}$ = 239 Hz, $Ar_{CF}$), 140.6 (m, $Ar_{CO}$), 105.1, 70.9, 70.8, 70.3, 69.6; HRMS calcd for $[M]^+$ $C_{28}H_{36}F_4O_{10}$ 608.2245, found 608.2224. Anal. Calcd for $C_{28}H_{36}F_4O_{10}$: C 55.26, H 5.90; found C 55.31, H 5.82.

***p*-Phenylene-35-crown-11 (22).** A solution of bis[2-[2-[2-[2-(*p*-toluenesulfonyl)ethoxy]ethoxy]ethoxy]ethoxy]benzene (4.50 g, 5.84 mmol) in dry THF (200 mL) was added to a refluxing suspension of diethylene glycol (0.62 g, 5.84 mmol) and NaH (0.42 g, 17.53 mmol) in dry THF (400 mL) under $N_2$ and stirred for 4 d. After cooling down to room temperature, the reaction mixture was quenched with $H_2O$. The solvent was removed to leave a solid residue which was dissolved in $CH_2Cl_2$ (150 mL) and washed with $H_2O$ (3 × 100 mL). The organic layer was dried ($MgSO_4$) and concentrated to a colorless oil which was purified by column chromatography ($SiO_2$, $CH_2Cl_2$/MeOH 100:2) to yield **22** as a white crystalline solid (464 mg, 15%): mp 55.0−56.0 °C; positive-ion electrospray MS *m/z* 550 $[M + NH_4]^+$; $^1H$ NMR ($CDCl_3$, 360 MHz) $\delta$ 6.85 (4H, s), 4.09 (4H, t), 3.84 (4H, t), 2.58−2.74 (32H, m); $^{13}C$ NMR ($CDCl_3$, 90 MHz) $\delta_C$ 153.1, 115.7, 70.7, 70.6, 70.6, 70.5, 70.5, 70.5, 70.5, 70.4, 69.7, 69.2. Anal. Calcd for $C_{26}H_{44}O_{11}$: C 58.63, H 8.33; found C 58.64, H 8.27.

**[2]Catenane 15·4PF$_6$.** A solution of **8** (234 mg, 0.39 mmol), **12**.2PF$_6$ (109 mg, 0.15 mmol), and **13** (45 mg, 0.17 mmol) in dry MeCN (7 mL) was stirred at room temperature for 5 d. The solvent was removed, and the resulting solid was purified by column chromatography ($SiO_2$, MeOH/2M $NH_4Cl$/$MeNO_2$ 7:2:1). After counterion exchange ($NH_4PF_6$/$H_2O$), the solid was recrystallized ($CH_3COCH_3$/$H_2O$) to yield **15**·4PF$_6$ as an orange/red crystalline solid (158 mg, 60%): mp > 250 °C decomposition; FABMS *m/z* 1708 $[M^+]$, 1563 $[M - PF_6]^+$, 1418 $[M - 2PF_6]^+$, 1273 $[M - 3PF_6]^+$: $^1H$ NMR ($CD_3CN$, 400 MHz) $\delta$ 8.95 (8H, d), 7.78 (8H, s), 7.76 (8H, d), 5.69 (4H, s), 3.98 (4H, t), 3.89 (8H, m), 3.83 (4H, t), 3.75 (4H, t), 3.68 (4H, t), 3.60 (4H, t), 3.57 (4H, s), 3.52 (4H, t); $^{19}F$ NMR ($CD_3CN$, 380 MHz, 236 K) $\delta_F$ −70.27 (d, $^1J_{FP}$ = 662 Hz, $PF_6^-$), −156.73 (s); $^{13}C$ NMR ($CD_3CN$, 90 MHz) $\delta_C$ 151.0, 146.8, 146.0, 137.6, 131.9, 126.3, 113.9, 75.0, 72.0, 71.8, 70.9, 70.7, 70.3, 67.7, 65.8; HRMS calcd for $[M - PF_6]^+$ $C_{64}H_{68}F_{22}N_4O_{10}P_3$ 1563.3797, found 1563.3731. Anal. Calcd for $C_{64}H_{68}F_{28}N_4O_{10}P_4$: C 44.96, H 4.01, N 3.28; found C 44.79, H 3.92, 3.28.

**[2]Catenane 16·4PF$_6$.** The procedure described for the preparation of **15**·4PF$_6$ was followed to yield **16**·4PF$_6$ as an orange/red crystalline solid (67 mg, 57%): mp >250 °C decomposition; FABMS *m/z* 1527 $[M - PF_6]^+$, 1382 $[M - 2PF_6]^+$, 1237 $[M - 3PF_6]^+$; $^1H$ NMR ($CD_3CN$, 400 MHz, 353 K) $\delta$ 8.97 (8H, d), 7.87 (8H, s), 7.74 (8H, d), 6.36 (2H, m, $J_{HF}$ = 10.5 Hz), 5.72 (8H, s), 3.88−4.00 (8H, m), 3.87 (4H, m), 3.76 (4H, m), 3.58−3.65 (16H, m), 3.57 (4H, s); $^{19}F$ NMR ($CD_3CN$, 340 MHz, 300 K) $\delta_F$ −66.0 (d, $^1J_{FP}$ = 728 Hz, $PF_6^-$), −132.7 (s); $^{13}C$ NMR ($CD_3CN$, 100 MHz) $\delta_C$ 151.0, 146.8, 145.7, 140.3, 137.5, 131.8, 129.7 (m, $J_{CF}$ = 203 Hz, $Ar_{CF}$), 126.3, 113.8, 104.8 (m, $Ar_{CO}$), 71.7, 71.4, 71.1, 70.8, 70.3, 70.3, 70.0, 67.6, 65.7; HRMS calcd for $[M - PF_6]^+$ $C_{64}H_{70}F_{20}N_4O_{10}P_3$ 1527.3986, found 1527.3995.

**Table 5.** Crystal Data, Data Collection, and Refinement Parameters[a]

| | **8** | **9** | **15**·4$PF_6$ | **16**·4$PF_6$ | **18**·4$PF_6$ |
|---|---|---|---|---|---|
| formula | $C_{28}H_{36}O_{10}F_4$ | $C_{28}H_{38}O_{10}F_2$ | $C_{64}H_{68}N_4O_{10}F_4$·4$PF_6$ | $C_{64}H_{70}N_4O_{10}F_2$·4$PF_6$ | $C_{64}H_{68}N_4O_{10}F_4$·4$PF_6$ |
| solvent | | | 4MeCN | 4MeCN·0.5$H_2O$ | 3MeCN·0.75MeOH·0.25$H_2O$ |
| formula weight | 608.6 | 572.6 | 1873.3 | 1846.3 | 1860.8 |
| color, habit | clear plates | clear needles | orange/red rhombus | red prisms | orange/red rhombus |
| crystal size (mm) | 0.50 × 0.33 × 0.17 | 0.77 × 0.37 × 0.17 | 0.50 × 0.50 × 0.17 | 0.50 × 0.23 × 0.10 | 0.47 × 0.40 × 0.23 |
| lattice type | monoclinic | monoclinic | triclinic | triclinic | triclinic |
| space group | $P2_1$ | $I2/a$ | $P\bar{1}$ | $P\bar{1}$ | $P\bar{1}$ |
| temperature (K) | 293 | 293 | 293 | 173 | 173 |
| $a$ (Å) | 8.370(2) | 18.885(4) | 14.049(6) | 13.550(1) | 13.859(2) |
| $b$ (Å) | 8.386(2) | 8.262(2) | 14.961(7) | 13.868(2) | 14.026(2) |
| $c$ (Å) | 21.150(9) | 18.931(6) | 22.690(13) | 26.895(3) | 26.330(1) |
| α (deg) | | | 80.17(4) | 83.86(1) | 92.35(1) |
| $\beta$ (deg) | 100.33(2) | 105.27(1) | 81.38(4) | 80.31(1) | 95.79(1) |
| $\gamma$ (deg) | | | 74.00(3) | 60.95(1) | 119.57(1) |
| $V$ (Å$^3$) | 1460.4(9) | 2849(1) | 4490(4) | 4353.1(9) | 4404(1) |
| $Z$ | 2 | 4[b] | 2 | 2 | 2 |
| $D_{calcd}$ (g cm$^{-3}$) | 1.384 | 1.335 | 1.385 | 1.409 | 1.403 |
| $F$(000) | 640 | 1216 | 1920 | 1898 | 1908 |
| radiation | Cu Kα | Mo Kα | Cu Kα | Cu Kα[c] | Cu Kα[c] |
| $\mu$ (mm$^{-1}$) | 1.04 | 0.11 | 1.80 | 1.82 | 1.84 |
| $\theta$ range (deg) | 1.5−63.0 | 2.2−25.0 | 2.0−50.0 | 1.7−55.0 | 1.7−57.5 |
| no. of unique reflections measured | 2544 | 2486 | 9201 | 10616 | 11996 |
| no. of unique reflections observed $\|F_o\| > 4\sigma(\|F_o\|)$ | 2298 | 928 | 5356 | 5016 | 7081 |
| absorption correction | empirical | none | none | none | none |
| maximum, minimum transmission | 0.93, 0.46 | | | | |
| no. of variables | 380 | 195 | 1017 | 1206 | 1188 |
| $R_1$[d] | 0.052[e] | 0.087 | 0.129 | 0.127 | 0.136 |
| $wR_2$[f] | 0.063[g] | 0.198 | 0.342 | 0.337 | 0.373 |
| weighting factors $a$, $b$[h] | 0.0005[i] | 0.047, 9.471 | 0.223, 17.810 | 0.298, 0.312 | 0.292, 4.738 |
| largest difference peak, hole (e Å$^{-3}$) | 0.49, −0.18 | 0.21, −0.20 | 0.55, −0.51 | 0.86, −0.44 | 0.98, −0.64 |

[a] Graphite-monochromated radiation, $\omega$ scans, Siemens P4 diffractometer, refinement based on $F^2$. Computations were carried out using the SHELXTL PC program system (SHELXTL PC version 5.03, Siemens Analytical X-Ray Instruments, Inc., Madison, WI, 1994). [b] The molecule has crystallographic $C_i$ symmetry. [c] Rotating anode source. [d] $R_1 = \sum||F_o| - |F_c||/\sum|F_o|$. [e] Refinement based on $F$. [f] $w^{-1} = \sigma^2(F_o^2) + (aP)^2 + bP$. [g] The value given is for $R_w$. [h] $wR_2 = \sqrt{\{\sum[w(F_o^2 - F_c^2)^2]/\sum[w(F_o^2)^2]\}}$. [i] The value given is $g$ in $w^{-1} = \sigma^2(F) + gF^2$.

**[2]Catenane 18·4PF$_6$. Method A.** The procedure described for the preparation of **15**·4$PF_6$ was followed to yield **18**·4$PF_6$ as an orange/red crystalline solid (6 mg, 3%): mp >250 °C decomposition; FABMS *m/z* 1563 [M − $PF_6$]$^+$, 1418 [M − 2$PF_6$]$^+$, 1273 [M − 3$PF_6$]$^+$; $^1$H NMR ($CD_3COCD_3$, 300 MHz) $\delta$ 9.38 (8H, d), 8.39 (8H, d), 8.03 (8H, s), 6.09 (8H, s), 5.50 (br m), 4.00−4.10 (16H, m), 3.85 (8H, m), 3.71 (8H, m); $^{19}$F NMR ($CD_3COCD_3$, 340 MHz, 213 K) $\delta_F$ −70.1 (d, $^1J_{FP}$ = 728 Hz, $PF_6^-$), −136.0 (s), −137.1 (s); $^{13}$C NMR ($CD_3CN$, 90 MHz) $\delta_C$ 147.8, 147.0, 146.3, 139.2, 137.0, 132.1, 126.2, 104.6, 71.3, 71.0, 70.3, 70.0, 66.3; HRMS calcd for [M − $PF_6$]$^+$ $C_{64}H_{68}F_{22}N_4O_{10}P_3$ 1563.3797, found 1563.3804. Anal. Calcd for $C_{64}H_{68}F_{28}N_4O_{10}P_4$: C 44.96, H 4.01, N 3.28; found C 44.71, H 3.91, N 3.12. **Method B.** A solution of **11** (159 mg, 0.26 mmol), **12**.2$PF_6$ (74 mg, 0.11 mmol), and **13** (30 mg, 0.12 mmol) in dry DMF (7 mL) was maintained at 12 kbar for 3 d. The reaction mixture was purified as described for method A to yield **18**·4$PF_6$ as an orange/red crystalline solid (43 mg, 24%) with physical and spectroscopic properties identical with those of a sample prepared by method A.

**[2]Catenane 23·4PF$_6$.** The procedure described for the preparation of **15**·4$PF_6$ was followed to yield **23**·4$PF_6$ as an orange/red crystalline solid (20 mg, 8%): mp >250 °C decomposition; FABMS 1632 [M$^+$], 1487 [M − $PF_6$]$^+$, 1342 [M − 2$PF_6$]$^+$, 1197 [M − 3$PF_6$]$^+$; $^1$H NMR ($CD_3CN$, 300 MHz, 297 K) $\delta$ 8.98 (8H, d), 7.87 (8H, d), 7.82 (8H, s), 5.75 (8H, s), 4.00 (4H, m), 3.93 (4H, m), 3.84 (4H, m), 3.77 (4H, m), 3.63 (8H, m), 3.58 (4H, s), 3.56 (4H, m), 3.48 (4H, m), 3.42 (4H, m), 3.33 (4H, m); $^{13}$C NMR ($CD_3CN$, 90 MHz) $\delta_C$ 147.5, 145.8, 137.6, 131.8, 126.8, 113.7, 71.7, 71.1, 71.1, 71.1, 70.4, 70.4, 70.4, 70.0, 69.6, 68.0, 65.7. HRMS calcd for [M − $PF_6$]$^+$ $C_{62}H_{76}F_{18}N_4O_{11}P_3$ 1487.4436, found 1487.4495.

**X-ray Crystallography.** Table 5 provides a summary of the crystal data, data collection and refinement parameters for **8**, **9**, **15**·4$PF_6$, **16**·4$PF_6$, and **18**·4$PF_6$.

**Molecular Modeling.** Molecular mechanics simulations were carried out using the AMBER* forcefield as implemented in Macromodel V. 5.0. *Ab initio* and AM1 semiempirical calculations were carried out using Spartan 4.1.1.[31] All calculations were performed on a Silicon Graphics Power Indigo2 workstation. The starting structures were assembled from the relevant X-ray crystal data and modified within Macromodel, and then fully minimized (final gradient <0.5 kJ/Å) using the Polak Ribiere Conjugate Gradient (PRCG) algorithm. Solvation (with extended cut-offs) was included in the form of the GB/SA solvation model for $H_2O$. AM1 Semiempirical calculations were carried out on the lowest energy conformers obtained from molecular mechanics calculations.

**Absorption, Luminescence, and Electrochemical Studies.** The measurements were performed as described previously.[9c,12] Experimental errors were as follows: absorption maxima ±2 nm, emission maxima ±2 nm, excited-state lifetimes ±10%, relative fluorescence intensity ±5%, electrochemical potentials ±10 mV.

**Acknowledgment.** This research was supported by the Engineering and Physical Sciences Research Council (EPSRC) as well as by Merck Sharp & Dohme in the UK. Financial support from the Italian MURST and University of Bologna (Funds for special projects) is also acknowledged. The work was carried out within the framework of the EU TMR Project FMRX-CT96-0076. We wish to acknowledge use of the EPSRC's Cambridge Structural Database through the EPSRC Chemical Database Service at Daresbury.

**Supporting Information Available:** Tables listing atomic coordinates, temperature factors, bond lengths and angles, and torsion angles and details of the refinement of the X-ray crystallographic data (36 pages). See any current masthead page for ordering information and Internet access instructions.

JA970640A

(31) Spartan V4.1, Wavefunction Inc., 18401 Von Karman Ave., 370 Irvine CA 92715.